JOURNAL OF INFORMATION AND COMMUNICATION TECHNOLOGY
https://e-journal.uum.edu.my/index.php/jict

How to cite this article:
Mohamed Shariff, M. A., Khairunnizam, N., & Jumaat, A. K. (2025). A convex variational interactive model with projection method for digital images partitioning. *Journal of Information and Communication Technology, 24*(3), 70-89. https://doi.org/10.32890/jict2025.24.3.4

A Convex Variational Interactive Model with Projection Method for Digital Images Partitioning

[1]Mohamed Ammareza Mohamed Shariff, [2]Nuruljannah Khairunnizam &
[*3]Abdul Kadir Jumaat
[1,2&3]School of Mathematical Sciences, Faculty of Computer and Mathematical Sciences, Universiti Teknologi MARA, Malaysia
[3]Institute for Big Data Analytics and Artificial Intelligence (IBDAAI), Universiti Teknologi MARA, Malaysia

[1]2021171857@student.uitm.edu.my
[2]2021119841@ student.uitm.edu.my
[*3]abdulkadir@tmsk.uitm.edu.my
*Corresponding author

Received: 26/3/2025 Revised: 30/6/2025 Accepted: 3/7/2025 Published: 31/7/2025

ABSTRACT

Digital image partitioning separates the foreground of an image from the background for subsequent analysis. In literature, the variational global model is frequently employed for digital images partitioning; however, it has been shown to underperform when the targeted object is situated near a neighbouring object. To address this issue, researchers recently devised the variational interactive model (VIM). However, because of the formulation's non-convexity, it is sensitive to the placement of the initial contour and provides inaccurate results if the initial contour is not positioned correctly. Consequently, a new convex formulation of VIM was recently developed based on the chessboard distance function, known as the Selective Segmentation based on Chessboard distance function (SSCD) model. Although this model achieved better accuracy and efficiency in image partitioning and is less sensitive to the initial contour's location compared to the non-convex VIM, the partitioning process is significantly slower, especially for large-sized images. This stems from the utilisation of a complex penalty term and the approximation of the regularisation term during the energy minimisation phase, which also impacts the accuracy of the partitioning results. This work contributes by proposing a new convex VIM that omits the penalty term and avoids approximating the regularisation term. Moreover,

the idea of utilising the projection method is proposed to speed up the partitioning process with improved accuracy. Numerical experiments demonstrated that the proposed model achieved higher accuracy and efficiency compared to existing models. The proposed model has the potential to be formulated into a three-dimensional formulation in the future.

Keywords: Convex formulation, image partitioning, interactive segmentation, projection method, variational interactive model.

INTRODUCTION

Image partitioning, also known as image segmentation, is a process of delineating an image into its individual objects or regions that allows it to be applied in many applications such as medical image analysis (Shewajo & Fante, 2023), pattern recognition, image understanding, and computer vision (Fang et al., 2021; Ikbal & Serap, 2023). Image partitioning can be defined as a process that divides a single digital image into several segments (Tan, 2016). There are five image partitioning techniques, which are thresholding, clustering, artificial neural network, edge-based, and region-based. Thresholding is a straightforward yet effective technique for image partitioning that helps distinguish the foreground from the background. According to Yogamangalam and Karthikeyan (2016), the thresholding procedure converts a multilayer image into a binary and selects the appropriate thresholding T to divide the image's pixels into distinct regions and distinguish between foreground and background items. However, thresholding has a well-known drawback of being sensitive to image noise.

The clustering technique divides an image into different classes without using any prior knowledge. When objects are divided into groups, the clustering process occurs that makes the objects within one group more similar to one another than to objects in another group (Sivachandiran, 2015). Hard clustering, k-means and fuzzy clustering are several types of clustering algorithms (Yogamangalam & Karthikeyan, 2016). However, the clustering method comes with limitations. According to Tyagi (2017), the k-means clustering method, a widely used clustering method in clustering analysis, is sensitive to images with noise. It also has no rules for choosing the K value, and sometimes issues a misclassification. Another method, known as the Fuzzy C-Mean Clustering (FCM), which is an improvement of the k-means algorithm, also faces the same issue as k-means clustering, as the main limit of the standard FCM is that it is sensitive to noise (Tyagi, 2017). The abnormal feature of the method, where the objective function does not take spatial information, tends to wrongly classify the noisy pixel.

In the artificial neural network (ANN) technique, different components (neurons) are tied to weights and connected via links (Sivachandiran, 2015). The technique develops knowledge in a manner similar to how the human brain works and is handled by specific examples rather than being programmed to perform a specific task. This approach begins by mapping an image into a neural network where each neuron represents a pixel. The state of each neuron is then guided towards the least energy prescribed by the neural network, while picture edges (the partitioning output) are retrieved using dynamic equations. However, according to Salvi et al. (2021), while ANNs are powerful tools for image analysis, there are also limitations to the method. For instance, deep networks are complex, as their parameters need an enormous amount of training, and a single layer within the deep network can be difficult to interact with. In addition, deep networks are highly reliant on the amount of data available (Azman et al., 2024). Consequently, they are generally represented as a black box that does not explain predictions in ways that a human can understand.

The edge-based technique describes a model that transforms original digital images into edge digital images and uses an edge detection function for the image partitioning process. Edges are important characteristics for image analysis because they are regions of rapid change in the image intensity function. A contour can be created by finding and connecting edges using edge detection. Some of the most often used edge detection operators include Prewitt, Roberts, Sobel, and Laplace. They typically entail creating curved line segments, or edges, from areas of discontinuity, according to research by Chakraborty et al. (2018). However, they usually exhibit excessive sensitivity to image noise, particularly when the noise is mistakenly detected as an image edge.

Region-based image partitioning techniques are built on continuity. By attempting to distinguish an object's pixels from their background pixels based on intensity, region-based partitioning techniques attempt to identify image edges between regions that satisfy various homogeneity requirements (Jumaat & Chen, 2019). Variational models are well-known region-based image partitioning techniques that have been shown to be efficient for partitioning an object's regions in many applications such as computer vision (Zhu et al., 2022), coronary arteries image segmentation (Gu et al., 2020), and colour medical and natural images (Yang et al., 2020). Additionally, as the variational models employ minimisation-based mathematical models that are capable of adapting to image topological changes, they are less sensitive to image noise compared to edge-based and clustering techniques. Additionally, they are not dependent on the amount of data, as no training is needed compared to ANN-based methods. Due to these strengths, variational models in digital image partitioning were the primary focus of this research.

There are two categories of variational models: global and interactive. The model that is capable of partitioning every object in an image based on predetermined attributes is known as the variational global model (VGM). The models developed by Zhi and Shen (2018), Gu et al. (2020), Yang et al. (2020) and Fang et al. (2021) are examples of VGMs. VGMs, however, are less effective in partitioning only a specific object from an image (Abdullah & Jumaat, 2022). To partition a particular object of an observed digital image, the variational interactive model (VIM) is more applicable. Effective VIMs include the models proposed by Rada and Chen (2012), Li et al. (2016), Fang et al. (2019), Liu et al. (2021) and Zhao et al. (2022). Although the models are capable of partitioning a specific object in an image, they are sensitive to the initial segmentation contour's location, as the formulations are developed in a non-convex framework. To address this gap, this study aims to formulate a new VIM, which is formulated in a convex framework, to partition a specific object in an image.

RELATED WORKS

VIM aims to partition a particular object within an observed digital image. In the image processing community, the interactive variational model is also known as the variational selective segmentation model. These models require the end user to be interactively involved in determining the targeted object by defining a set of markers around it. The models will utilise the marker set to achieve an accurate result. A subset of target objects or regions of interest in an image is partitioned using this model (Zhao et al., 2022). Partitioning a specific object in a digital image is important in many applications, such as in medical settings, especially in tumour shape analysis, surgical planning, robotics, and biometric identification. There are many existing VIMs in the literature. However, due to the non-convexity of the formulations, they are sensitive to the placement of the initial contour, resulting in inaccuracy if the initial contour is improperly located in the images. To address the issue, researchers reformulated the VIMs in a convex framework. Key studies in this area are summarised in Table 1, which highlights their strengths and limitations and provides context for the development of the proposed new VIM.

Table 1

Comparative Overview of Existing Convex VIMs

Author (Year)	Segmentation Model	Strength	Limitation
Spencer and Chen (2015)	Convex Distance Selective Segmentation (CDSS)	A convex model with a segmentation speed of approximately 200 seconds per image, based on a comparative study by Jumaat and Chen (2019)	Slow segmentation due to the presence of a penalty term and the approximation process for the regularisation term
Jumaat and Chen (2019)	Dual Selective Segmentation (DUSS)	A convex model without a penalty term, which results in a faster segmentation process. The model is approximately 33 times faster than the CDSS model	Segmentation is slow for large image sizes due to the approximation process of the regularisation term
Abdullah and Jumaat (2022)	Selective Segmentation based on Chessboard distance function (SSCD)	A convex model using a chessboard distance function, achieving a segmentation speed of approximately 100 seconds per image	Slow segmentation due to the presence of a penalty term and the approximation process for the regularisation term

Based on Table 1, the earliest convex VIM was the Convex Distance Selective Segmentation (CDSS), proposed by Spencer and Chen (2015). However, Jumaat and Chen (2019) found that the CDSS model was slow due to the existence of a computationally expensive penalty term in the model. Consequently, they proposed the Dual Selective Segmentation (DUSS) model to eliminate the penalty term. They also demonstrated that the formulation was based on a special case of the piecewise constant, where it was limited to only two phases, which represented the foreground and background of the provided image. In addition, the formulation of DUSS was convex, which made the model independent of the contour's initialisation. Results demonstrated that the DUSS was about 33 times faster than the CDSS model.

Another idea to improve the speed of the CDSS model was proposed by Abdullah and Jumaat (2022) through the formulation of the Selective Segmentation based on Chessboard distance function (SSCD) model by changing the Euclidean distance used in the CDSS model to the Chessboard distance function. According to Lee and Horng (1996), the general expression of the Euclidean distance is more difficult, which slows down the experimentation compared to the Chessboard distance function. Additionally, the Chessboard distance produced less errors compared to the Euclidean distance (Chen et al., 2004). In terms of computing efficiency and the precision of the segmentation outcomes, the SSCD model exhibited better performance compared to the CDSS model. Nevertheless, the SSCD model utilised a similar penalty term to that used in the CDSS model, which made the formulation computationally expensive. Consequently, more processing time was needed to complete the image partitioning process, especially for large image sizes. On top of that, all convex VIMs mentioned above employed an approximation process of the regularisation term during the energy minimisation phase. This resulted in the partitioning process becoming slower, especially for large-sized images and affected the accuracy of the partitioning results.

Based on the problems above, this study proposed a new convex VIM termed the Convex Selective Segmentation (CSS), which is convex and utilises the Chessboard distance function in the formulation without the penalty term. To further speed up the partitioning process, a projection method originally proposed by Chambolle (2004) for the image denoising task was utilised to solve the proposed CSS model. The following section outlines the methodology employed in the study. The next section addresses the analysis and results, whereas the final section covers the conclusion and recommendations.

METHODOLOGY

This section discusses the research methodology for the proposed model. Figure 1 illustrates the framework of the methodology phases involved in this study.

Figure 1

Framework of the Research Methodology

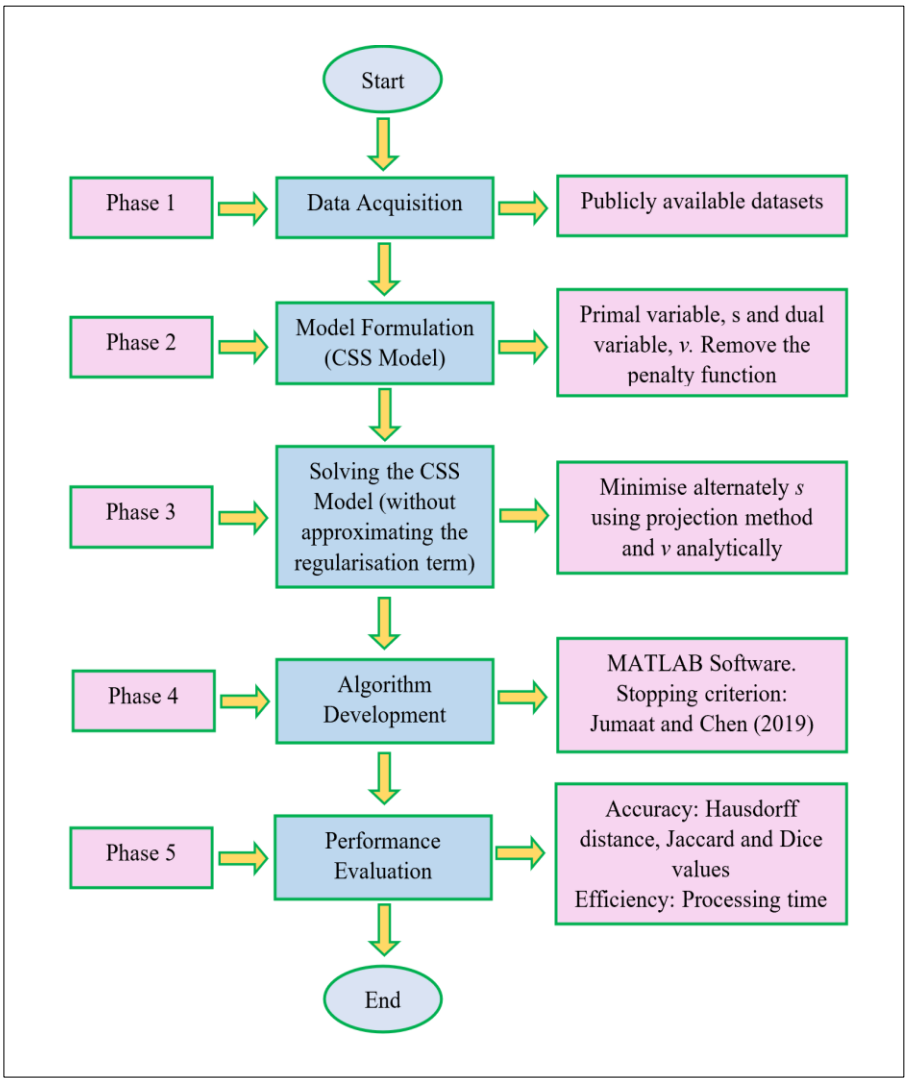

There were five phases involved in this study, as illustrated in Figure 1. The first phase was data acquisition from available databases. Next was the formulation of the proposed CSS model. All the steps to solve the proposed model are explained in detail in the next phase. After that, a MATLAB algorithm was developed to implement the model. Finally, the proposed model's image partitioning results were compared to those of the existing models. The subsequent subsection provides a detailed explanation of each phase.

Data Acquisition

Data acquisition was the first phase in this study. This study involved three representative medical imaging modalities as case studies. The first case involves brain tumour segmentation using magnetic resonance imaging (MRI) data obtained from Cheng (2017). The second case study focuses on mammographic breast mass segmentation using images from Moreira et al. (2012). The third case uses ultrasound images of breast masses from Rodtook et al. (2018). The images were selected because they were challenging to be partitioned due to the existence of noise, blurred edges, low contrast and different grey levels of intensity which reflect fundamental challenges commonly encountered in various information and communication technology (ICT) based image analysis tasks, including document analysis, security surveillance, satellite imaging, and industrial quality control. Thus, the segmentation strategies developed and validated here are applicable to any ICT domain where accurate partitioning of grayscale images is needed. In addition, the benchmark images, which are essential for comparing and evaluating different models, were also retrieved from the same sources for this study. Each dataset had four images selected from it, making a total of twelve test images.

Model Formulation

In this study, the SSCD model proposed by Abdullah and Jumaat (2022) was considered. The SSCD model was a modified version of the CDSS model from Spencer and Chen (2015). In the SSCD model, a set of markers, also known as a geometrical constraint, *A* was utilised, located near the targeted object and formed a polygon P such that the point $(x_P, y_P) \in P$. The distance energy term, $D = \int_\Omega P_{CD}\, s\, d\Omega$ was formulated in a level set function $s(x,y) \in [0,1]$ in an image $z = z(x,y)$ of domain Ω such that the point $(x,y) \in \Omega$. The level set function $s(x,y)$ represented the partitioning result either in binary representation or contour (curve) representation. The Chessboard distance $P_{CD}(x,y)$ was defined as $P_{CD}(x,y) = \max(|x - x_p|, |y - y_p|)$. Thus, the SSCD models were given as the following Equation 1.

$$\min_s \left\{ SSCD(s, g_1, g_2) = \int_\Omega |\nabla s|_E \, d\Omega + \int_\Omega g s \, d\Omega + \theta \int_\Omega P_{CD} s \, d\Omega + \alpha \int_\Omega q(s) d\Omega \right\} \quad (1)$$

The first term was the regularisation term with the coefficient E as the edge detector used to smooth the segmentation result and stop the partitioned contour at the image edge during the partitioning process. The function $g = (g_1 - z)^2 - (g_2 - z)^2$ in the second term was the fitting function to ensure the partitioning contour fit the input image where g_1 was the average intensity inside the partitioning contour while g_2 was the average intensity outside the partitioning contour. The third term, the distance energy term, was utilised to capture a specific object in the image. The final term weighted by α was the penalty function from Spencer and Chen (2015) to ensure the solution was bounded within 0 and 1.

It was defined as $q(s)=\left[\sqrt{(2s-1)^2+\varepsilon}-1\right]\left[\frac{1}{2}+\frac{1}{\pi}\arctan\left(\frac{\sqrt{(2s-1)^2+\varepsilon}-1}{\varepsilon}\right)\right]$ with $\varepsilon \approx 0$. The SSCD model was solved using the Additive Operator Splitting (AOS) method introduced by Spencer and Chen in 2015. Although the SSCD model achieved better accuracy and efficiency in partitioning a moderate-sized image compared to the CDSS model, the partitioning process became significantly slower, especially for large-sized images. The first reason was due to the application of AOS to solve the model where the regularisation term $|\nabla s|_E$ was approximated so as $\lambda \approx 0$ to avoid singularity problem. Secondly, the penalty function, $q(s)$ in the last term of the model was computationally expensive. Besides affecting the efficiency, these problems also reduced the accuracy of the partitioning result.

To address the limitations of the SSCD model, this study proposes a new convex VIM, namely CSS, by introducing the dual variable in the original formulation of the SSCD model in Equation 1. This idea allowed the penalty function in the SSCD model to be removed (Jumaat & Chen, 2019). Therefore, the SSCD model was reformulated to obtain the proposed CSS model defined as in Equation 2:

$$\min_{s,v\in[0,1]}\left\{CSS(s,v)=\int_\Omega |\nabla s|_E\, d\Omega+\int_\Omega gv\, d\Omega+\theta\int_\Omega P_{CD}v\, d\Omega+\frac{1}{2\gamma}\int_\Omega (s-v)^2\, d\Omega\right\} \tag{2}$$

Note that Equation 2 involves two variables that need to be solved, namely the primal variable *s* and the dual variable *v* that will be discussed later. To demonstrate the convexity of the proposed CSS model, we first let $CSS(s,v)=F(s,v)+G(s,v)$, such that $F(s,v)=\frac{1}{2\gamma}\int_\Omega (s-v)^2 d\Omega$ and $G(s,v)=R(s)+\int_\Omega (g+\theta P_{CD})v\, d\Omega$ where $R(s)=\int_\Omega |\nabla s|_E\, d\Omega$. The function $\int_\Omega (g+\theta P_{CD})v\, d\Omega$ (dependent only on *v*) was convex as deduced from the work by Spencer and Chen (2015). According to Boyd and Vandenberghe (2004), a function $f:\mathbb{R}^n\to\mathbb{R}$ is said to be convex if for all $x,y\in\mathbb{R}^n$ and for all $\psi\in[0,1]$, the inequality $f(\psi x+(1-\psi)y)\le\psi f(x)+(1-\psi)f(y)$ holds. Therefore, to show that $R(s)$ and $F(s,v)$ are convex, let s_1, s_2, s_3 and s_4 be any functions in bounded variation ($s_1, s_2, s_3, s_4\in BV(\Omega\subset\mathbb{R}^n)$) such that $s_1\neq s_2\neq s_3\neq s_4$. By definition of convexity given by Boyd and Vandenberghe (2004), we arrived at the following Equation 3 for the function $R(s)$ as follows:

$$\begin{aligned} R\left(\psi s_1+(1-\psi)s_2\right) &= \int_\Omega \left|\nabla\left(\psi s_1+(1-\psi)s_2\right)\right|_E d\Omega \\ &= \int_\Omega \left|\psi\nabla s_1+(1-\psi)\nabla s_2\right|_E d\Omega \\ &\le \psi\int_\Omega |\nabla s_1|_E\, d\Omega+(1-\psi)\int_\Omega |\nabla s_2|_E\, d\Omega \\ &= \psi R(s_1)+(1-\psi)R(s_2) \end{aligned} \tag{3}$$

Similarly, the function $F(s,v)$ can be represented by the following Equation 4:

$$\begin{aligned} F\left[\psi\left(s_1,s_2\right)+\left(1-\psi\right)\left(s_3,s_4\right)\right] &= F\left[\psi s_1+\left(1-\psi\right)s_3,\psi s_2+\left(1-\psi\right)s_4\right] \\ &= \frac{1}{2\gamma}\int_\Omega\left[\psi s_1+\left(1-\psi\right)s_3-\psi s_2-\left(1-\psi\right)s_4\right]^2 d\Omega \\ &= \frac{1}{2\gamma}\int_\Omega\left[\psi\left(s_1-s_2\right)+\left(1-\psi\right)\left(s_3-s_4\right)\right]^2 d\Omega \\ &\le \frac{1}{2\gamma}\psi\int_\Omega\left(s_1-s_2\right)^2 d\Omega+\frac{1}{2\gamma}\left(1-\psi\right)\int_\Omega\left(s_3-s_4\right)^2 d\Omega \\ &= \psi F\left(s_1,s_2\right)+\left(1-\psi\right)F\left(s_3,s_4\right). \end{aligned} \tag{4}$$

Equations 3 and 4 demonstrated that the functions $R(s)$ and $F(s,v)$ satisfied the definition of a convex function. Since the sum of two convex functions was convex, the function $CSS(s,v)=F(s,v)+G(s,v)$, which represented the proposed CSS model in Equation 2, was convex.

Solving the CSS Model

In order to solve the proposed CSS model of Equation 2, the energy minimisation concept was utilised. CSS was minimised independently with regard to s and v to determine the minimiser, which was then iterated until convergence. Thus, the following minimising problems were taken into consideration:

i) Firstly, with the fixed v, the following Equation 5 of the functional CSS with respect to s was minimised:

$$\min_s\left\{CSS=\int_\Omega\left|\nabla s\right|_E d\Omega+\frac{1}{2\gamma}\int_\Omega(s-v)^2 d\Omega\right\} \tag{5}$$

ii) Secondly, assuming that s was fixed, the following Equation 6 of the functional CSS with respect to v was minimised:

$$\min_v\left\{CSS=\int_\Omega gv\,d\Omega+\theta\int_\Omega P_{CD}v\,d\Omega+\frac{1}{2\gamma}\int_\Omega(s-v)^2 d\Omega\right\} \tag{6}$$

To solve Equation 5 without approximating the regularisation term, this study proposed the use of the projection method by Chambolle (2004). The projection method was originally developed to address the issue of image denoising and was regarded as an effective and quick solution. This study demonstrated how to apply the projection method for the image partitioning problem in solving Equation 5.

In order to apply the projection method to our proposed image partitioning model, the gradient and divergence operators were defined as follows:

The gradient operator with image size $M(i,j)$:

$$(\nabla s)_{i,j} = \left((\nabla s)^1_{i,j}, (\nabla s)^2_{i.j}\right)$$
$$(\nabla s)^1_{i,j} = \begin{cases} s_{i+1,j} - s_{i,j} & \text{if } i < M \\ 0 & \text{if } i = M \end{cases}$$
$$(\nabla s)^2_{i,j} = \begin{cases} s_{i,j+1} - s_{i,j} & \text{if } j < M \\ 0 & \text{if } j = M \end{cases}$$

The divergence operator dual variable $q = (q_1 \cdot q_2)$:

$$(\nabla \cdot q)_{i,j} = \begin{cases} q^1_{i,j} - q^1_{i-1,j} & \text{if } 1 < i < M \\ q^1_{i,j} & \text{if } i = 1 \\ -q^1_{i-1,j} & \text{if } i = M \end{cases} + \begin{cases} q^2_{i,j} - q^2_{i,j-1} & \text{if } 1 < j < M \\ q^2_{i,j} & \text{if } j = 1 \\ -q^2_{i,j-1} & \text{if } j = M \end{cases}$$

Thus, following the work from Chan et al. (1999) and Chambolle (2004), Equation 5 can be written as Equation 7:

$$\max_{|q| \le E} \min_{s} \int_{\Omega} s \nabla \cdot q + \frac{1}{2\gamma}(s - v)^2 \, d\Omega \tag{7}$$

The minimisation with respect to *s* resulted in the following Equation 8:

$$\nabla \cdot q + \frac{1}{\gamma}(s - v) = 0 \Rightarrow s = v - \gamma \nabla \cdot q \tag{8}$$

Upon substituting Equation 8 into 7, the following Equation 9 was obtained:

$$\max_{|q| \le E} \int_{\Omega} (v - \gamma \nabla \cdot q) \nabla \cdot q + \frac{\gamma}{2}(\nabla \cdot q)^2 \, d\Omega \tag{9}$$

which can be simplified to the following Equation 10:

$$\max_{|q| \le E} \int_{\Omega} v \nabla \cdot q - \frac{\gamma}{2}(\nabla \cdot q)^2 \, d\Omega \tag{10}$$

Variation of energy of Equation 10 with relation to the vector field *q* resulted in the following Equation 11:

$$\int_{\Omega} (-\nabla v + \gamma \nabla (\nabla \cdot p)) \cdot \delta q \, d\Omega \tag{11}$$

The optimality condition was provided together with the point-wise constraint $|q|^2 - E^2 \leq 0$ as in Equation 12:

$$-\nabla(\gamma\nabla \cdot q - v) + rq = 0 \tag{12}$$

The function $r \geq 0$ was denoted as the Lagrange multiplier. As demonstrated by Chambolle (2004), Equation 12 can be written as Equation 13:

$$|\nabla(\gamma\nabla \cdot q - v)|^2 - r^2 E^2(x) = 0 \tag{13}$$

where $r = \frac{1}{E}|\nabla(\gamma\nabla \cdot q - s)|$. Using this information, we arrived at the following Equation 14 as follows:

$$-\nabla(\gamma\nabla \cdot q - v) + \frac{1}{E}|\nabla(\gamma\nabla \cdot q - v)|q = 0 \tag{14}$$

For the solution of Equation 14, we employed the semi-implicit gradient descent with a time step δt (Chambolle, 2004). The result is given in Equation 15 as follows:

$$q^{n+1} = \frac{q^n + \delta t\nabla(\nabla \cdot q^n - v/\gamma)}{1 + \frac{\delta t}{E}|\nabla(\nabla \cdot q^n - v/\gamma)|} \tag{15}$$

Now, to solve Equation 6, an analytical approach could be used, which resulted in Equation 16:

$$v = \min\{\max\{s(x) - \gamma g - \gamma\theta P_{CD}, 0\}, 1\} \tag{16}$$

Algorithm Development

We applied the alternating minimisation approach to solve the CSS model in Equation 2, where we first solved Equation 5, followed by Equation 6 alternately, until the stopping criterion was met. In this study, we adopted the stopping criterion from Jumaat and Chen (2019) defined as $\max\left(\frac{\|s_n - s_{n-1}\|}{\|s_{n-1}\|}, \frac{\|v_n - v_{n-1}\|}{\|v_{n-1}\|}\right) < tol$ where n is the number of iteration, the tolerance value, $tol = 10^{-5}$ and maximum iteration, $maxit = 5000$. The image partitioning process of the CSS model terminated when the relative change in both the primal variable s and the dual variable v fell below the specified tolerance, tol or when the number of iterations exceeded $maxit$. All calculations were implemented using the MATLAB R2017b software. The MATLAB algorithm, as shown in Algorithm 1, outlines the steps involved in the implementation process.

Algorithm 1. The Algorithm to Solve the CSS Model

1. Load the input image in MATLAB using 'imread' command.
2. Set values of *tol*= 10^{-5}, *maxit=5000,* $\gamma = 0.09$, $\delta t = 0.0001$ and specify the marker set.
3. Set θ = [1000, 5000] depending on the input images. The value of θ is large if the targeted object is close to the neighbouring objects.
4. Compute the image edge, *E* and the Chessboard distance $P_{CD}(x, y)$.
5. Define the initial contour *s* that is generated by the marker set.
6. Initialise iteration counter *n*=1.
7. Repeat until convergence or maximum iterations:
   a) Evolve *s* according to Equation 8 and 15 to obtain s_n.
   b) Update *v* using Equation 16.
   c) Check for convergence:

If $\max\left(\frac{\|s_n - s_{n-1}\|}{\|s_{n-1}\|}, \frac{\|v_n - v_{n-1}\|}{\|v_{n-1}\|}\right) < tol$ then stop (converged). Otherwise, if $n >$ *maxit*, stop (maximum iterations reached).

   d) Increment $n \leftarrow n+1$

Performance Evaluation

In the final phase, the performance accuracy of the model was evaluated using Jaccard coefficient (JC), Dice coefficient (DC), and Hausdorff distance (H), similarly to what was done in Azman et al. (2024). The formula for Jaccard was $JC = |S_d \cap S_*| / |S_d \cup S_*|$ while the formula for Dice was $DC = |S_d \cap S_*| / |S_d| + |S_*|$ where S_d was the set of partitioned domains of the targeted object and S_* was the true set of the targeted object. The return value of the similarity function was between 0 and 1. The closer the result value to 1, the higher the level of perfection of the image partitioning result. The formula for H was $H(S_d, S_*) = max\left(\sup_{a \in S_d} \inf_{b \in S_*} k(a,b), \sup_{b \in S_*} \inf_{a \in S_d} k(a,b)\right)$ where $k(a,b)$ was the Euclidean distance between *a* and *b*. The smaller the H (approach to zero), the more accurate the image partitioning result. The efficiency of the model was analysed by computing the processing time in MATLAB.

ANALYSIS AND RESULTS

Two sets of experiments are presented in this section to compare our new model to existing models. Using the DUSS, SSCD and CSS models, we conducted an image partitioning comparison on three case studies where each case study consisted of four test images in Experiment 1. Two models with higher accuracy were chosen to be compared in Experiment 2. Experiment 2 depicts the experiment on partitioning different sizes of images using the chosen models.

Experiment 1: Image Partitioning Comparison of DUSS, SSCD and CSS Models

In Experiment 1, test images from the MRI of brain tumour (first case study), mammographic breast masses (second case study), and ultrasound breast masses datasets (third case study) obtained from online databases were partitioned by the new proposed CSS model and the existing DUSS and SSCD

models. All twelve test images were of size 128 x 128 pixels. The results in partitioning the MRI of brain tumour, mammographic breast masses and ultrasound breast masses are displayed in Figures 2, 3 and 4, respectively.

Figure 2

Image Partitioning Results on MRI Brain Tumour Images

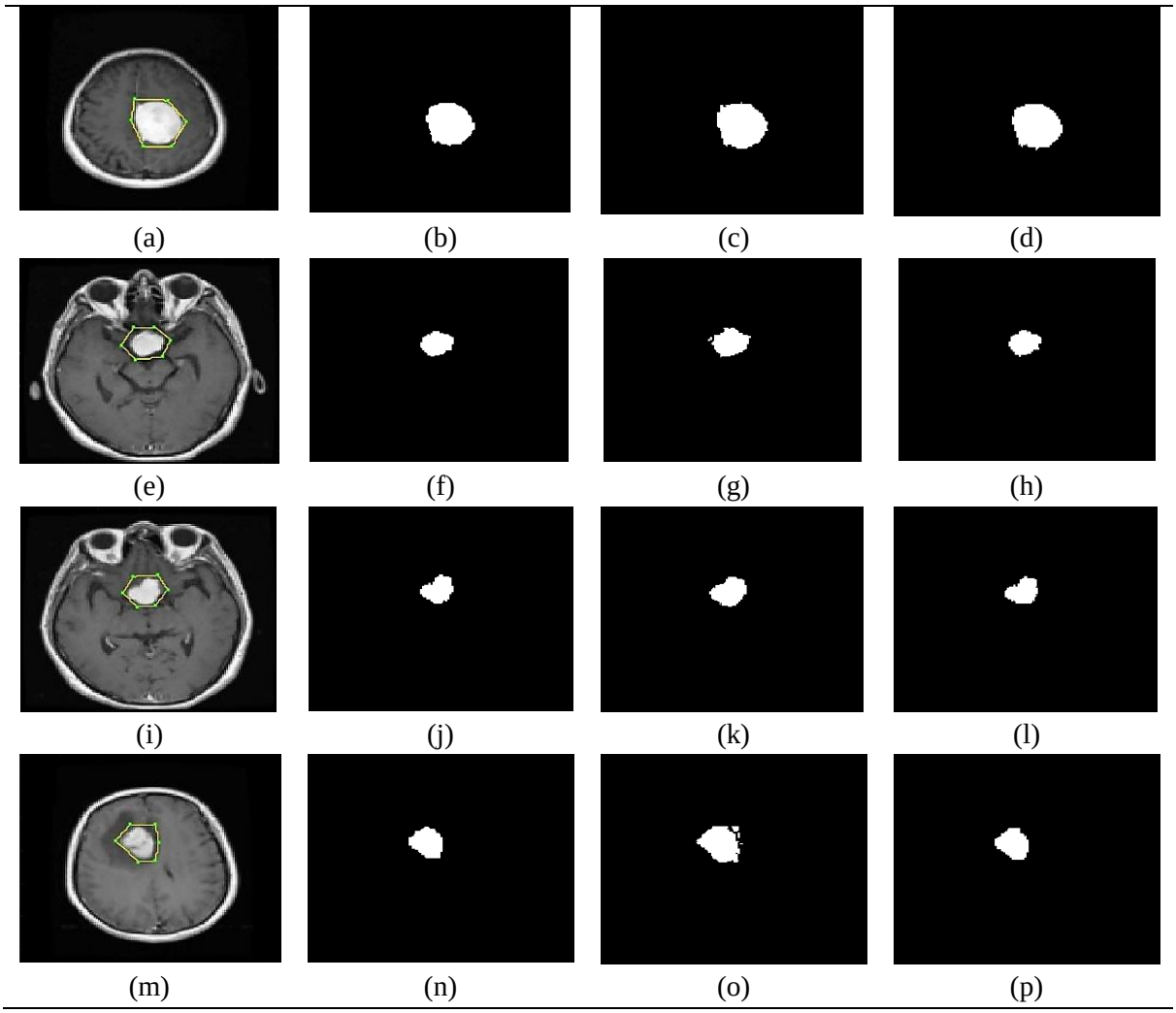

Figure 3

Image Partitioning Results on Mammographic Breast Mass Images

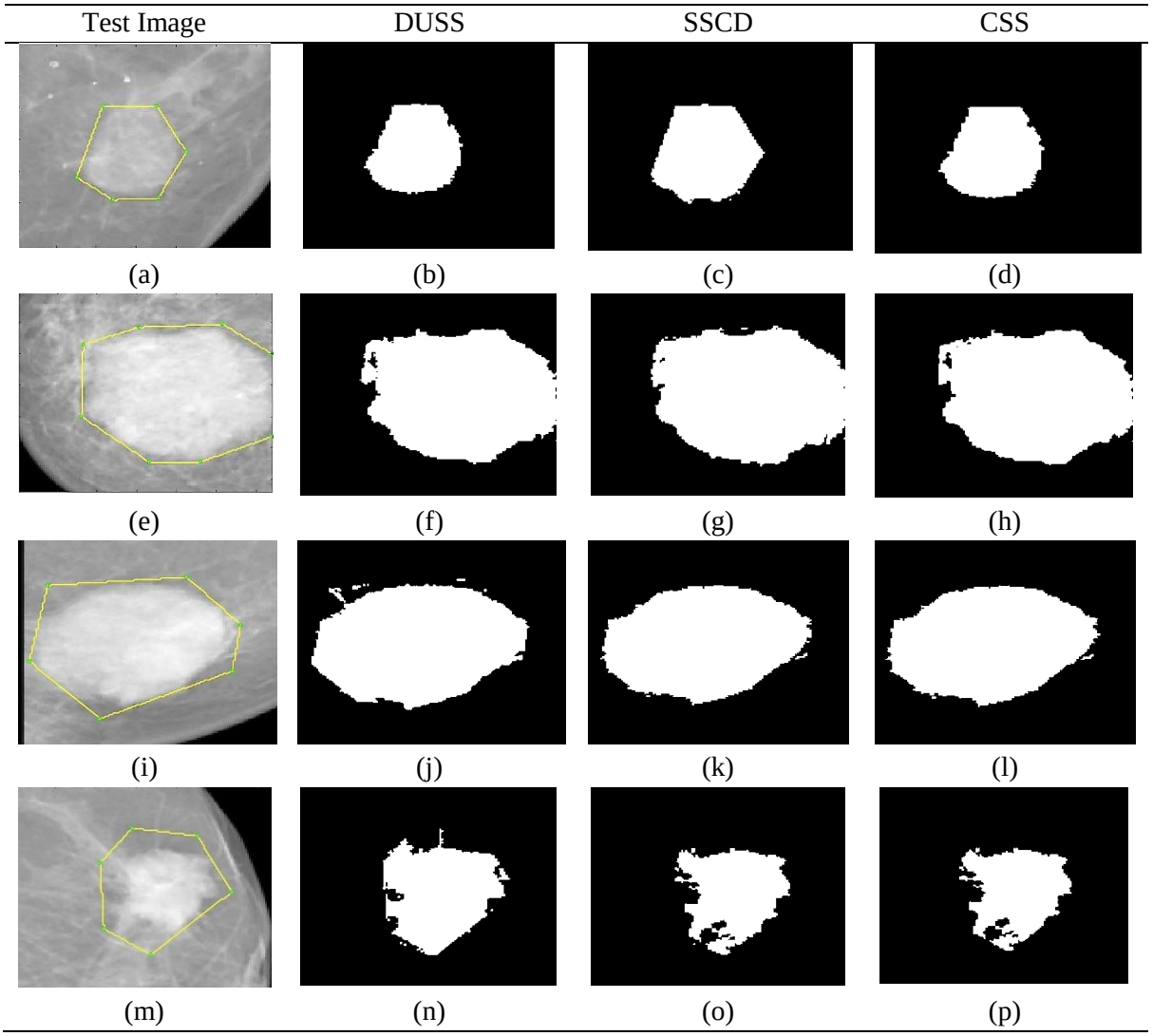

Figure 4

Image Partitioning Results on Ultrasound Breast Mass Images

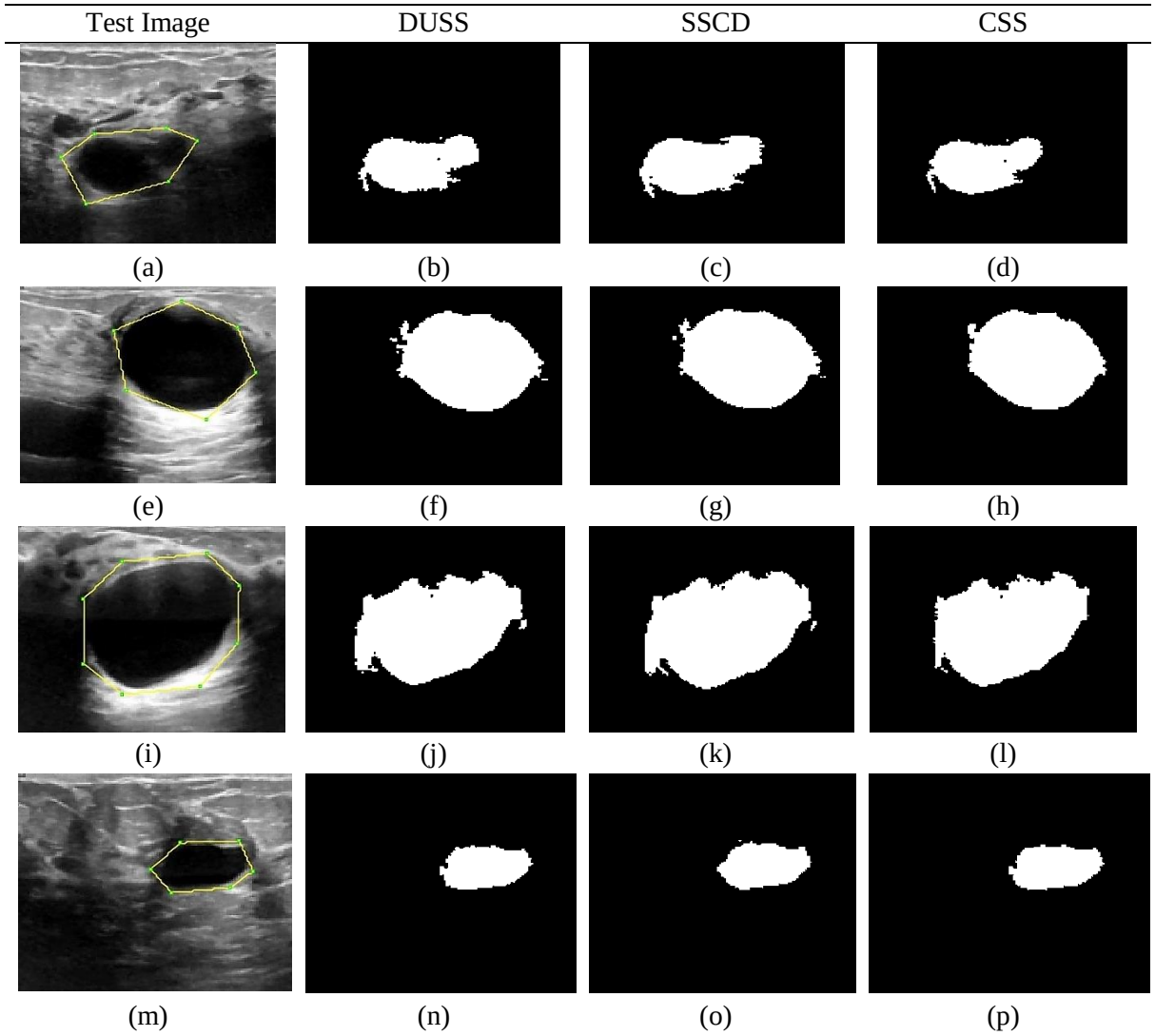

Based on Figures 2, 3 and 4, the first column represents the test images with the set of markers in green and the initial partition contour in yellow. This is followed by the second, third and fourth columns that represent the partitioning results in binary form generated by DUSS, SSCD and the proposed CSS model, respectively. According to Figures 2, 3 and 4, all models were capable of capturing all targeted objects. However, the image partitioning results obtained from the DUSS and SSCD models showed noticeable over-segmentation in several cases when compared to the proposed CSS model. Over-segmentation refers to the inclusion of undesired regions outside the intended object boundaries, often caused by sensitivity to nearby structures with similar intensity levels. This issue is particularly evident in Figures 2(g), 2(o), Figures 3(j), 3(n), and Figures 4(f), 4(g), 4(j), and 4(k), where the DUSS and SSCD models failed to fully suppress adjacent background regions, especially when the target object was close to other anatomical structures or exhibited blurred boundaries. In contrast, the CSS model produced more accurate delineations with tighter adherence to the true object boundaries, demonstrating its improved selectivity and robustness against background interference. For quantitative analysis, we provided the values of average processing time, H, JC and DC in the following Figure 5.

Figure 5

The Average Values of Processing Time, H, DC and JC for All Models

The experimental results presented in Figure 5 provide a comparison of three image partitioning models: DUSS, SSCD, and CSS, evaluated based on their average processing time in Figure 5(a), H in Figure 5(b), DC in Figure 5(c), and JC in Figure 5(d). These metrics are critical in assessing the trade-off between computational efficiency and segmentation accuracy. The processing time for each model demonstrates significant differences in computational efficiency. The CSS model achieved the lowest processing time at 7.448 seconds, followed by DUSS at 25.471 seconds, whereas SSCD exhibited the highest processing cost at 172.507 seconds. This indicated that CSS was approximately 23 times and 3 times faster than the SSCD and DUSS model, respectively or 71% faster than DUSS and 95.7% faster than SSCD, making it the most computationally efficient model.

H is a critical metric for assessing boundary accuracy, where lower values indicate better performance. Based on Figure 5(b), CSS achieved the lowest H value at 5.126, outperforming DUSS (5.974) and SSCD (7.148). This signifies that CSS reduced the segmentation boundary deviation by 14.2% compared to DUSS and by 28.3% compared to SSCD, reinforcing its better performance in boundary preservation. The DC and JC are widely used metrics for evaluating segmentation accuracy. Higher

values indicate better model performance. Based on Figure 5(c), CSS attained the highest DC at 0.940, marginally outperforming DUSS (0.935) and significantly surpassing SSCD (0.909). This improvement translated to a 3.4% accuracy gain over SSCD. A similar pattern can be observed in Figure 5(d), where the proposed CSS achieved the highest JC at 0.888, followed closely by DUSS (0.880) and SSCD (0.835). CSS exhibited a 6.35% higher Jaccard score than SSCD, while DUSS remained 5.4% superior to SSCD.

From Experiment 1, we can conclude that CSS was the optimal model and achieved a better balance between computational efficiency and segmentation accuracy. This indicated the effectiveness of using the regularisation term without approximation in solving our model through the projection method. Additionally, introducing the dual variable in the formulation to replace the high computational penalty term was capable of increasing the efficiency of the proposed CSS model. The results also indicated that the DUSS model achieved the second-highest segmentation accuracy, while SSCD demonstrated clear limitations of efficiency and accuracy. In the next experiments, we were interested in further comparing our CSS model with the chosen DUSS model using different image sizes.

Experiment 2: Testing Different Image Sizes for DUSS and CSS Models

In Experiment 2, both DUSS and CSS models were tested with different image sizes of 64×64, 128×128, 256×256 and 512×512 pixels. A sample brain tumour dataset was used in this experiment. Figure 6 shows the output images of the experiment.

Figure 6

Image Partitioning Results on Different Image Sizes for DUSS and CSS Models

Image Size	64×64 (4,096 unknowns)	128×128 (16,384 unknowns)	256×256 (65,536 unknowns)	512×512 (262,144 unknowns)
DUSS	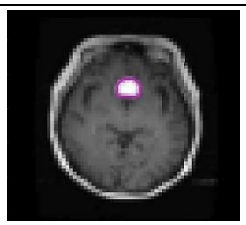	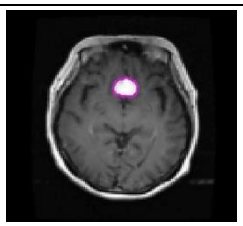	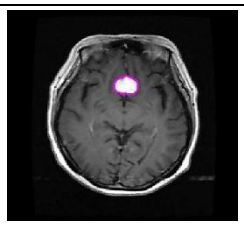	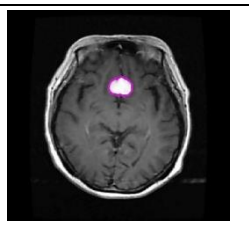
CSS	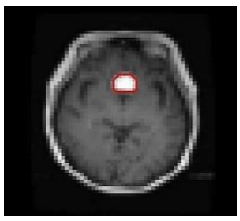	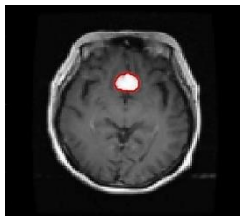	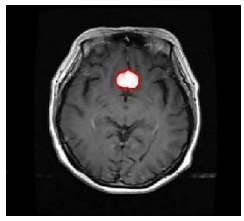	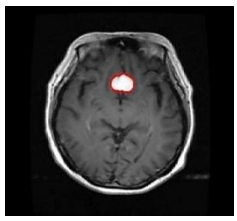

Figure 6 presents a qualitative comparison of the segmentation results in contour form obtained using the DUSS and CSS models across different image resolutions. All models were capable of partitioning all the targeted objects in the images. Quantitative results demonstrated that both DUSS and the proposed models had similar accuracy values of H=1, JC=0.8065 and DC=0.8929. In addition to accuracy, computational efficiency was a critical factor in evaluating the image partitioning models. Figure 7 illustrates the processing time required by each model at different image sizes.

Figure 7

The Average Processing Time (s) at Different Image Sizes for DUSS and CSS Models

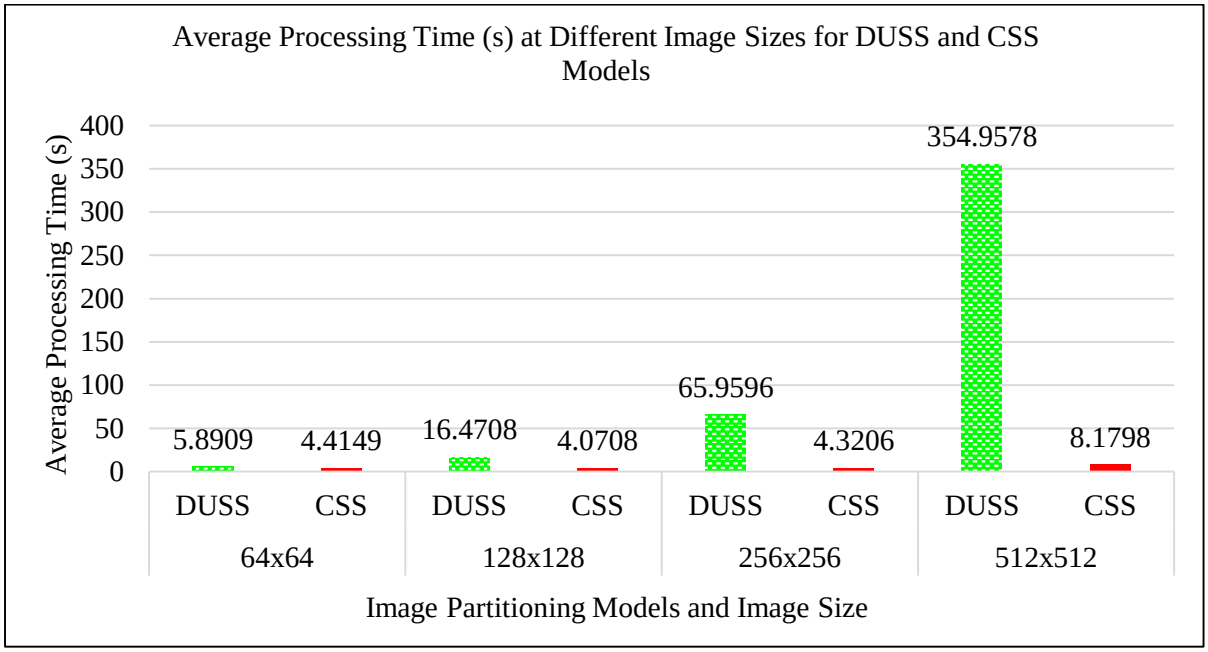

Figure 7 revealed that CSS significantly outperformed DUSS in terms of speed. For images of size 128 × 128, the CSS model was approximately 4.05 times faster than DUSS, reducing the processing time by 75.3%. As the image size increased to 256 × 256, CSS maintained its efficiency and processed the image 15.27 times faster than DUSS, corresponding to a 93.45% reduction in execution time. The computational advantage became even more pronounced at higher resolutions, where for 512 × 512 images, CSS was 43.39 times faster, achieving 97.69% reduction in processing time. These findings indicated that while both models achieved effective segmentation, the computational cost of DUSS increased exponentially, whereas CSS scaled efficiently with image size.

The primary explanation for the outcomes in Experiments 1 and 2 was the approach of neglecting the penalty function in the proposed CSS model. Furthermore, the application of the projection method enabled the solution of the CSS model to be computed without the need to approximate the regularisation term. Conversely, the DUSS and SSCD models incorporated a penalty function, and both models were resolved by approximating the regularisation term, which decreased the effectiveness and efficiency of their outcomes.

Overall, the CSS model demonstrated better segmentation accuracy and significantly improved computational efficiency. It consistently preserved sharper boundaries, reduced image partitioning errors and improved localisation accuracy. Furthermore, the substantial reduction in processing time, particularly for high-resolution images, underscores the scalability of CSS, making it a suitable choice for many applications such as medical imaging applications, remote sensing, robotic vision and satellite or aerial imagery.

CONCLUSION

The focus of this study was to formulate a new convex VIM termed the CSS model. This new model adopted the chessboard distance function and the dual variable ideas to replace the Euclidean distance and the penalty term respectively to reduce the complexity of the CSS model. Since the existing models approximated the regularisation term to deal with the singularity problem, we proposed using the projection method to address the issue. Thus, the CSS model was capable of being solved without the approximation of the regularisation term. To compare the performance of the existing model with the CSS model, two different experiments were used. Experiment 1 compared the image partitioning results from the existing DUSS and SSCD models with the proposed CSS model. Results indicated that the CSS model achieved the highest accuracy and efficiency, followed by the DUSS model and finally the SSCD model. In Experiment 2, we chose the DUSS model to be compared with the CSS model to partition different sizes of images. The numerical experiment indicated that while both models achieved effective segmentation, the CSS model significantly outperformed DUSS in terms of efficiency. The primary limitation of the suggested CSS model was the necessity of employing a trial-and-error methodology to select an ideal combination of parameters involved in the formulation to get satisfactory results. Additionally, while the model performed well on grayscale medical images, preliminary testing indicated that its performance may degrade when segmenting extremely noisy images. Furthermore, while the current study focused on two-dimensional grayscale images, scalability to three-dimensional or colour image data presents computational and formulation challenges. Handling volumetric data would require an efficient extension of the dual variable formulation and projection method in higher dimensions, which remains an open area of research. Likewise, the generalisability of the CSS model to other domains such as natural images, satellite imagery, or industrial visual inspection requires further validation on diverse datasets with varying characteristics and noise models. Future work may focus on automating the parameter selection process using optimisation or learning-based methods, extending the model to support three-dimensional and colour image segmentation and validating its applicability across broader ICT domains. Developing robust failure detection mechanisms and adaptive strategies to handle noisy, low-contrast or texture-rich images is also a promising direction.

ACKNOWLEDGMENT

The authors extend their sincere gratitude to Universiti Teknologi MARA (UiTM) for supporting this research. This research received no specific grant from any funding agency in the public, commercial, or not-for-profit sectors.

REFERENCES

Abdullah, S. A., & Jumaat, A. K. (2022). Selective image segmentation models using three distance functions. *Journal of Information and Communication Technology*, *21*(1), 95–116. https://doi.org/10.32890/jict2022.21.1.5

Azman, N. F., Jumaat, A. K., Badarul Azam, A. S., Mohd Ghani, N. A. S., Maasar, M. A., Laham, M. F., & Nek Abd Rahman, N. (2024). Digital medical images segmentation by active contour model based on the signed pressure force function. *Journal of Information and Communication Technology, 23*(3), 393419. https://doi.org/10.32890/jict2024.23.3.2

Boyd, S., & Vandenberghe, L. (2004). *Convex optimisation*. Cambridge University Press.

Chakraborty, T., Saini, V., Govila, D., & Singh, G. (2019). Four most life threatening urogenital cancer and its management. *International Journal of Pharmaceutical Sciences and Research*, *9*(8), 3166–3174. https://doi.org/10.13040/IJPSR.0975-8232.9(8).3166-74

Chambolle, A. (2004). An algorithm for total variation regularization and denoising. *Journal Math. Imaging*, *20*(1–2), 89–97. http://dx.doi.org/10.1023/B: JMIV.0000011325.36760.1e

Chan, T., Golub, G., & Mulet, P. (1999). A nonlinear primal-dual method for total variation-based image restoration. *SIAM J. Sci. Comput*., *20*(6), 1964–1977. https://doi.org/10.1137/ S1064827596299767

Chen, Q., Yang, X., & Petriu, E. M. (2004). Watershed segmentation for binary images with different distance transforms. In A. E. Saddik & R. Goubran (Eds.), *The 3rd IEEE International Workshop on Haptic, Audio and Visual Environments and Their Applications* (pp. 111–116). IEEE. https://doi.org/10.1109/ HAVE.2004.1391891

Cheng, J. (2017). Brain tumor dataset (Version 5). figshare. https://doi.org/10.6084/m9.figshare. 1512427.v5

Fang, J., Liu, H., Zhang, L., Liu, J., & Liu, H. (2019). Active contour driven by weighted hybrid signed pressure force for image segmentation. *IEEE Access*, *7*, 97492–97504. https://doi.org/ 10.1109/ACCESS.2019.2929659

Fang, J., Liu, H., Zhang, L., Liu, J., & Liu, H. (2021). Region-edge-based active contours driven by hybrid and local fuzzy region-based energy for image segmentation. *Information Sciences*, *546*, 397–419. https://doi.org/10.1016/j.ins.2020.08.078

Gu, J., Fang, Y., Gao, Y., & Tian, F. (2020). Segmentation of coronary arteries images using global feature embedded network with active contour loss. *Computerised Medical Imaging and Graphics*, *86*, 101799. https://doi.org/10.1016/j.compmedimag.2020.101799

Ikbal, Y. M., & Serap, G. (2023). Recognition of Hereford and Simmental cattle breeds via computer vision. *Iranian J. Appl. Animal Sci.*, *13*(1), 21–32. https://journals.iau.ir/article_699902. html?lang=en

Jumaat, A. K., & Chen, K. (2019). A reformulated convex and selective variational image segmentation model and its fast multilevel algorithm. *Numerical Mathematics*, *12*(2), 403–437. https://doi.org/10.4208/nmtma.OA-2017-0143

Lee, Y. H., & Horng, S. J. (1996). The chessboard distance transform and the medial axis transform are interchangeable. In M. E. Kavanaugh (Ed.), *Proceeding of International Conference on Parallel Processing* (pp. 424–428). IEEE. https://doi. org/10.1109/IPPS.1996.508090

Li, B. N., Qin, J., Wang, R., Wang, M., & Li, X. (2016). Selective level set segmentationusing fuzzy region competition. *IEEE Access*, *4*, 4777–4788. https://doi.org/10.1109/ACCESS.2016. 2590440

Liu, H. X., Fang, J. X., Zhang, Z. J., & Lin, Y. C. (2021). Localised edge-region-based active contour for medical image segmentation. *IET Image Processing*, *15*(7), 1567–1582. https://doi.org/10.1049/ipr2.12126

Moreira, I. C., Amaral, I., Domingues, I., Cardoso, A., Cardoso, M. J., & Cardoso, J. S. (2012). INbreast: Toward a full-field digital mammographic database. *Academic Radiology*, *19*(2), 236–248. https://doi.org/10.1016/j.acra.2011.09.014

Rada, L., & Chen, K. (2012). A new variational model with dual level set functions for selective segmentation. *Communications in Computational Physics*, *12*(1), 261–283. https://doi.org/ 10.4208/cicp.190111.210611a

Rodtook, A., Kirimasthong, K., Lohitvisate, W., & Makhanov, S. S. (2018). Automatic initialisation of active contours and level set method in ultrasound images of breast abnormalities. *Pattern Recognition*, *79*, 172–182. https://doi.org/10.1016/j.patcog.2018.01.032

Salvi, M., Acharya, U. R., Molinari, F., & Meiburger, K. M. (2021). The impact of pre- and post-image processing techniques on deep learning frameworks: A comprehensive review for digital pathology image analysis. *Computers in Biology and Medicine, 128*, 104129. https://doi.org/10.1016/j.compbiomed.2020.104129

Shewajo, F. A., & Fante, K. A. (2023). Tile-based microscopic image processing for malaria screening using a deep learning approach. *BMC Medical Imaging*, *23*(1), 1-14. https://doi.org/10.1186/s12880-023-00993-9

Sivachandiran, S. (2015). Image Segmentation. *IEEE International Conference on Image Processing*, *1*(2), 345–348. https://doi.org/10.17816/byusu201511299-101

Spencer, J., & Chen, K. (2015). A convex and selective variational model for image segmentation. *Communications in Mathematical Sciences*, *13*(6), 1453–1472. https://doi.org/10.4310/CMS.2015.v13.n6.a5

Tan, Y. (2016). *GPU-based Parallel Implementation of Swarm Intelligence Algorithms*. Morgan Kaufmann. https://doi.org/10.1016/C2015-0-02468-6

Tyagi, L. (2017). Review of various image segmentation techniques. *International Journal of Engineering Research & Technology*, *30*(4), 440–443. https://doi.org/10.17577/IJERTV3IS040480

Yang, Y., Jia, W., & Wu, B. (2020). Simultaneous segmentation and correction model for color medical and natural images with intensity inhomogeneity. *The Visual Comput.*, *36*, 717–731. https://doi.org/10.1007/s00371-019-01651-4

Yogamangalam, R., & Karthikeyan, B. (2016). Segmentation techniques comparison in image processing. *International Journal of Engineering and Technology*, *5*(1), 307–313.

Zhao, W., Wang, W., Feng, X., & Han, Y. (2022). A new variational method for selective segmentation of medical image. *Signal Processing*, *190*, 108292. https://doi.org/10.1016/j.sigpro.2021.108292

Zhi, X. H., & Shen, H. B. (2018). Saliency driven region-edge-based top down level set evolution reveals the asynchronous focus in image segmentation. *Pattern Recognit.*, *80*, 241–255. https://doi.org/10.1016/j.patcog.2018.03.010

Zhu, G. L., Lv, X. G., Li, F., & Sun, X. M. (2022). Nonconvex variational approach for simultaneously recovering cartoon and texture images. *J. Electron. Imaging*, *31*(4), 043021. https://doi.org/10.1117/1.JEI.31.4.043021